Birefringence switching of Bragg gratings in fibers with internal electrodes

Zhangwei Yu[1,3], O. Tarasenko[2,3], W. Margulis[2,3]* and P. -Y. Fonjallaz[2,3]

[1]*JORCEP [Joint Research Centre of Photonics of the Royal Institute of Technology (Sweden) and Zhejiang University], Zhejiang University, Hangzhou 310058, China*
[2]*Acreo AB, Electrum 229, SE-164 40 Kista, Sweden*
[3]*Kista Photonics Research Center, Royal Institute of Technology, Electrum 229, SE-164 40 Kista, Sweden*
**Corresponding author: Walter.Margulis@acreo.se*

Abstract: A fiber Bragg grating was written in a side-hole fiber with internal metal alloy electrodes. The initial geometrical birefringence of this fiber gives rise to two Bragg resonances separated by 43 pm. Nanosecond risetime current pulses of up to 23 A were applied to the metal electrode, which heated and expanded rapidly. This caused mechanical stress in the fiber on a nanosecond scale, resulting in a negative shift of the Bragg wavelength peak for the fast axis mode, and positive but smaller shift for the slow axis mode. The fast change increased the peak separation to ~ 143 pm, corresponding to an increase in birefringence from 4.0×10^{-5} to 1.3×10^{-4}. Both peaks subsequently experienced a red-shift due to the relaxation of mechanical stress and the increasing core temperature transferred from the metal in many microseconds. Simulations give accurate description of the experimental results.

OCIS codes: (060.3735) Fiber Bragg gratings; (060.4005) Microstructured fibers.

References and links

1. H. M. Xie, Ph. Dabkiewicz, R. Ulrich, and K. Okamoto, "Side-hole fiber for fiber-optic pressure sensing," Opt. Lett. **11**, 333-335 (1986).
2. M. Turpin, M. Brevignon, J. P. Le. Pesant, and O. Gaouditz, "Interfero-polarimetric fiber optic sensor for both pressure and temperature measurement," in *Proceedings of IEEE Conference on Optical Fiber Sensors* (Institute of Electrical and Electronic Engineers, New York, 1992), pp. 362-365.
3. W. J. Bock, M. S. Nawrocka, and W. Urban´ czyk, "Highly sensitive fiber-optic sensor for dynamic pressure measurements," IEEE Trans. Instrum. Meas. **50,** 1085-1088 (2001).
4. S. Kreger, S. Calvert, and E. Udd, "High pressure sensing using fiber Bragg grating written in birefringent side hole fiber," in *Proceedings of IEEE Conference on Optical Fiber Sensors*, (Portland, 2002), pp. 355-358.
5. R. J. Schroeder, T. Yamate, and E. Udd, "High pressure and temperature sensing for the oil industry using fiber Bragg gratings written onto side hole single mode fiber," Proc. SPIE **3746,** 72-74 (1999).
6. T. Yamate, R. T. Ramos, R. J. Schroeder, and E. Udd, "Thermally insensitive pressure measurements up to 300 degrees C using fiber Bragg gratings written onto side-hole single mode fiber," Proc. SPIE **4185,** 628-631 (2000).
7. E. Chmielewska, W. Urbanczyk, and W. J. Bock, "Measurement of pressure and temperature sensitivities of a Bragg grating imprinted in a highly birefrigent side-hole fiber," Appl. Opt. **42**, 6284-6291 (2003).
8. C. Jewart, K. P. Chen, B. McMillen, M. M. Bails, S. P. Levitan, J. Canning, and I. V. Avdeev, "Sensitivity enhancement of fiber Bragg gratings to transverse stress by using microsturctural fibers," Opt. Lett. **31**, 2260-2262 (2006).
9. L. -E. Nilsson, Z. Yu, O. Tarasenko, H. Knape, P. -Y. Fonjallaz, and W. Margulis, "High-speed switching in fibres with electrodes," in *Proceedings of IEEE Conference on Transparent Optical Networks* (Rome, 2007), pp. 232-233.
10. Z. Yu, W. Margulis, O. Tarasenko, H. Knape, and P.-Y. Fonjallaz, "High-speed control of fiber Bragg gratings," in *Bragg Gratings, Photosensitivity, and Poling in Glass Waveguides*, OSA Technical Digest (CD) (Optical Society of America, 2007), paper JWA44.
11. Z. Yu, W. Margulis, O. Tarasenko, H. Knape, and P. -Y. Fonjallaz, "Nanosecond switching of fiber Bragg gratings," Opt. Express **15**, 14948-14953 (2007).
12. Z. Yu, W. Margulis, P.-Y. Fonjallaz, and O. Tarasenko, "Physics of electrically switched fiber Bragg gratings," in *Conference on Lasers and Electro-Optics/Quantum Electronics and Laser Science Conference and Photonic Applications Systems Technologies*, OSA Technical Digest Series (CD) (Optical Society of America, 2007), paper CMK1.

#94010 - $15.00 USD Received 18 Mar 2008; revised 19 May 2008; accepted 19 May 2008; published 21 May 2008

13. M. Fokine, L. E. Nilsson, Å. Claesson, D. Berlemont, L. Kjellberg, L. Krummenacher, and W. Margulis, "Integrated fiber Mach-Zehnder interferometer for electro-optic switching," Opt. Lett. **27,** 1643-1645 (2002).
14. J. A. Viator, S. Kreger, M. W. Winz, and E. Udd, "Modeling and experimental strain measurements on a non-homogeneous cylinder under transverse load," Proc. SPIE **5384**, 199-205 (2004).
15. R. Gafsi and M. A. El-Sherif, "Analysis of Induced-Birefringence Effects on Fiber Bragg Gratings," Opt. Fiber Technol. **6**, 299-323 (2000).
16. N. F Borrelli and R. A. Miller, "Determination of the individual strain-optic coefficients of glass by an ultrasonic technique," Appl. Opt. **7**, 745-750 (1968).
17. H. Knape and W. Margulis, "All-fiber polarization switch," Opt. Lett. **32**, 614-616 (2007).

1. Introduction

Side-hole fibers have the advantage of high sensitivity to pressure and low sensitivity to temperature [1-4]. Fiber Bragg gratings (FBG) imprinted in side-hole fibers have been shown to be good candidates for simultaneous sensing hydrostatic pressure and temperature [5-7]. Recently Kreger, *et al.*, [8] has reported that when the static transverse load was applied perpendicular or parallel to the direction of the two air holes, the direction orthogonal to the two holes suffered a much larger stress or strain, and the polarization parallel to the two holes has a larger wavelength shift. However, to the best of our knowledge, there is no published report on high-speed dynamic measurements of pressure and temperature in these special fibers until now. The potential application of high-speed polarization/wavelength switching in fiber lasers makes these studies particularly relevant.

In our previous work [9-11], we reported that a FBG component based on a side-hole fiber with internal electrodes has shown nanoseconds full off-on and on-off switching. Nanosecond high current pulses heated the metal electrodes and caused rapid metal expansion. As a consequence, the grating wavelength was blue-shifted (~-27 pm) for the fast axis mode, while it was red-shifted for the slow axis mode (~+5 pm). Besides, a much slower wavelength red-shift (many microseconds) as high as ~+17 pm was obtained for both polarizations. Furthermore, we demonstrated that the fast and slow wavelength shifts depend quadratically on the electrical pulse voltage and linearly on the pulse duration for the fast axis mode [12], i.e. depend linearly on the amount of energy deposited.

In this Paper, we further investigate the birefringence dynamic changes of side-hole fibers with internal electrodes. The FBG used show to be an excellent tool to reveal the amplitude and sign of the mechanical and thermal perturbations, and the ensuing time evolution of the birefringence. The simulation results are consistent with the experimental dynamic measurements.

2. Experiment

The 125 μm-thick silicate side-hole fiber had characteristics similar to those of the standard telecom fiber (core diameter 8.4 μm and $\Delta n = 0.0056$) but with two 28.8 μm-diameter holes running parallel to the core. The core-hole separation (edge-to-edge) was 13.4 μm. Figure 1(a) shows the cross section of the fiber used. Pieces of fiber were filled with 7 cm-long BiSn alloy (melting temperature 137°C) that occupy the entire cross-section of the holes [13]. The length of the alloy-filled holes and the core-hole separation were such that insertion loss was experimentally measured to be < 0.2 dB and the polarization-dependent loss < 0.1 dB. Both ends of the metal-filled fiber were free from metal to allow for convenient low-loss splicing.

A 4 cm-long Hamming-apodized FBG was written along the middle section of BiSn-filled fiber, with the holes aligned perpendicular to the UV beam incidence direction [11]. The grating was annealed in the oven at 100 °C for 12 hours. Due to the intrinsic geometrical birefringence of the fiber with internal metal electrodes, the grating has two reflection peaks at different wavelengths corresponding to the differing effective refractive indices for the two orthogonal polarization modes in this fiber. The reflection peak at the shorter wavelength takes place in the fast axis mode (x-axis), the one at the longer wavelength in the slow axis mode (y-axis). The identification of the axes is discussed in the simulations below. At room temperature, the Bragg wavelengths of the two polarizations are 1547.230nm and 1547.273nm, with a separation of 43 pm corresponding to a refractive index difference of

#94010 - $15.00 USD Received 18 Mar 2008; revised 19 May 2008; accepted 19 May 2008; published 21 May 2008

~4.0×10^{-5}. This is roughly one order of magnitude lower than in typical high-birefringence fibers. The 3-dB bandwidth and the reflectivity of both peaks are 44 pm and 75%, respectively.

After writing the gratings, electrical contacts were made from the side of the fiber at both extremities of the electrode. The grating was mounted on an aluminum substrate and covered with heat conductive, electrically isolating epoxy. Heat dissipation allows switching the devices at a few kHz with minor average drift of polarization. The resistance of the components was typically 43 Ω for a BiSn device with 7 cm active length. This value implies in a small impedance mismatch between the device and the 50 Ω coaxial cable transporting the high voltage (i.e., current) pulses. Electrical SMA contacts were used and a 0.1Ω resistive probe was connected in series with the 43 Ω loads for monitoring purposes.

A pulse generator consisting of a high voltage dc power supply and a high speed switch was employed for the driving pulses. The switch here was a low repetition rate spark gap circuit delivering 2 ns rise-time current pulses with the maximum switching voltage 3 kV and duration 10-241 ns determined by the cable length used. The light source was a tunable external cavity diode laser with which 1 pm wavelength resolution measurements are possible. Different input polarization states were selected with a polarization controller. A circulator, 3-dB splitter, high-speed photodiode, Ando AQ6317B optical spectrum analyzer and oscilloscope completed the experimental set-up, schematically illustrated in Fig. 1(b).

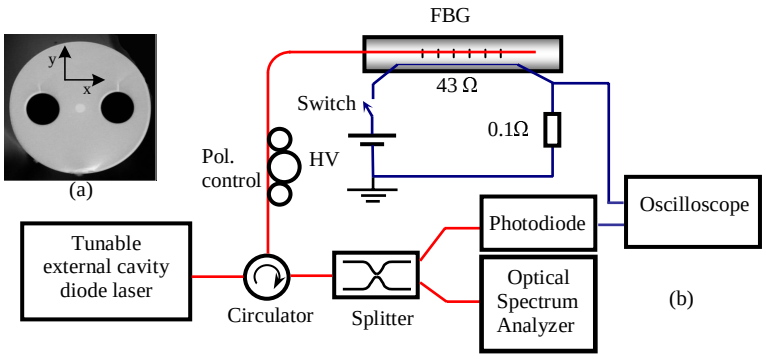

Fig. 1. (Color online) (a) Cross section of the two-hole fiber used here (SEM picture).
(b) The schematic of the system for dynamic measurements of the two polarization states.

Dynamic measurements were performed for the fast axis mode by properly aligning the input polarization and by tuning the external cavity laser source to the grating reflectivity maximum before the application of the current pulse. The changes in reflectivity as a function of time can be studied from the oscilloscope trace following the electrical excitation (Fig. 2(a)). Figure 2(b) schematically illustrates that the grating wavelength shifts in the above process can be divided into fast part (in tens of nanoseconds) and slow part (hundreds of microseconds). The former is due to mechanical stress created during the electrical pulse action, while the latter is due to the relaxation of mechanical stress and the slow increase of temperature in the core transferred from the metal electrode after each electrical pulse. The fast part corresponds to the initial reduction of the reflection of the grating at the probe wavelength (from t_0 to t_1). It reaches its maximum absolute value ($\Delta\lambda_M^x$) at instant t_1 ~241 ns, equal to the current pulse duration. Then the slow part takes effect: the grating gradually moves back with the decreasing mechanical stress and the increasing temperature in the core. The grating passes its original spectral position at instant t_2 ~68 μs and red-shift continues. At t_3 ~270 μs, the maximum positive $\Delta\lambda_{T+M}^x$ is reached, where the core temperature is near its maximum. After several milliseconds (t_4), the grating returns to its original spectral position again, since the mechanical stress is released and the component is back to room temperature. It should be mentioned that the identification of the behavior schematically illustrated in Fig. 2(b) (and in Fig. 2(d) below) involved experimentally examining the response of the device for various other probe wavelengths, as discussed in Ref. [11].

#94010 - $15.00 USD Received 18 Mar 2008; revised 19 May 2008; accepted 19 May 2008; published 21 May 2008

Similarly, dynamic measurements were also carried out for the slow axis mode, shown in a typical experimental trace (Fig. 2(c)) and the schematic diagram (Fig. 2(d)). Note that, now a positive and smaller wavelength shift happens during the electrical pulse duration and reaches its maximum ($\Delta\lambda_M^y$) at instant t_1 ~241 ns. Then, the relaxation of the mechanical stress blue-shifts the spectrum of the grating, while the increasing temperature in the core red-shifts the grating peak. In the beginning, the former dominates and the Bragg wavelength moves back a little until instant t_2 is attained at ~16 μs. Afterwards, the heat reaching the core dominates, so the grating continues to red-shift. The maximum positive spectral shift ($\Delta\lambda_{T+M}^y$) occurs at instant t_3 ~190 μs. Finally, the grating also returns to its original spectral position after instant t_4 ~20 ms. Full (100%) on-off switching is not achieved for this axis even with the highest current level (~23A) applied here, corresponding to an electrical pulse energy ~5 mJ/pulse.

The values of $\Delta\lambda_M$ and $\Delta\lambda_{T+M}$ depend on the pulse voltage and the pulse duration. Experimental data of the fast wavelength shift for both polarization states ($\Delta\lambda_M^x$ and $\Delta\lambda_M^y$) at different voltages are shown with blue and red squares in Fig. 3(a), for pulses with duration 241 ns. The absolute value of $\Delta\lambda_M^x$ is ~3.2 times larger than $\Delta\lambda_M^y$. Similarly, experimental data of the slow wavelength shift ($\Delta\lambda_{T+M}^x$ and $\Delta\lambda_{T+M}^y$) at different voltages are shown in Fig. 3(b) with blue and red squares. Here, $\Delta\lambda_{T+M}^y$ is larger than $\Delta\lambda_{T+M}^x$.

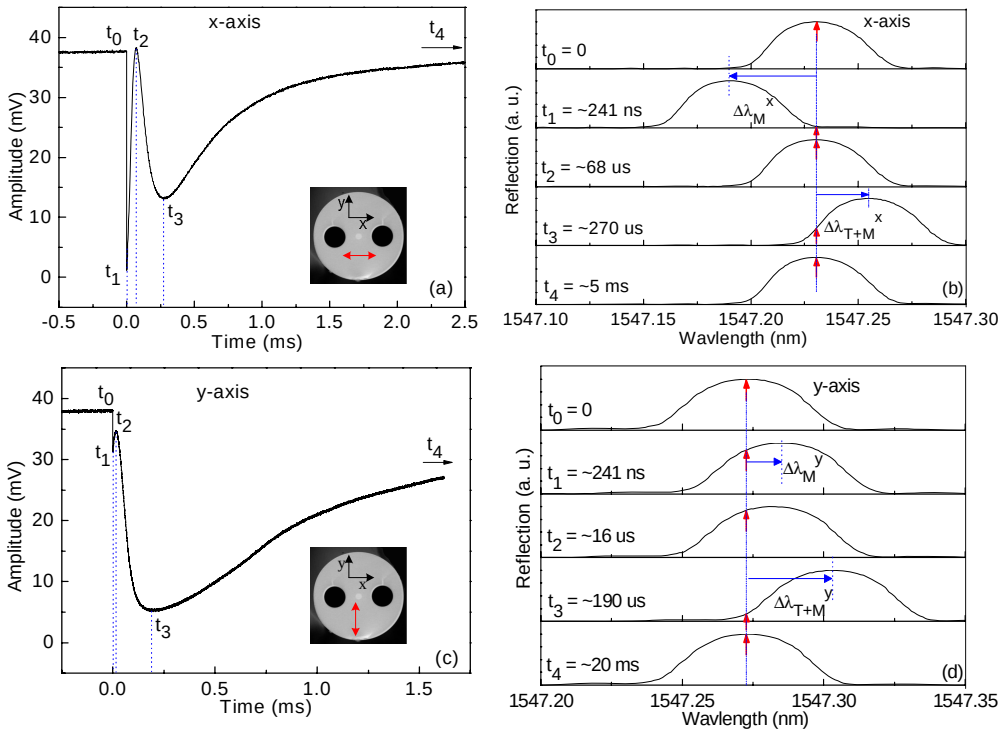

Fig. 2. (Color online) (a) Time evolution of the signal reflected by the FBG for probe light polarized along the x-axis. (b) Schematic illustration of the wavelength shift at various times. (c) Time evolution of the signal reflected by the FBG for probe light polarized along the y-axis. (d) Schematic illustration of the wavelength shift at various times. The red arrows in Figs. (b) and (d) indicate the wavelength of the tunable laser source during the measurement.

#94010 - $15.00 USD Received 18 Mar 2008; revised 19 May 2008; accepted 19 May 2008; published 21 May 2008

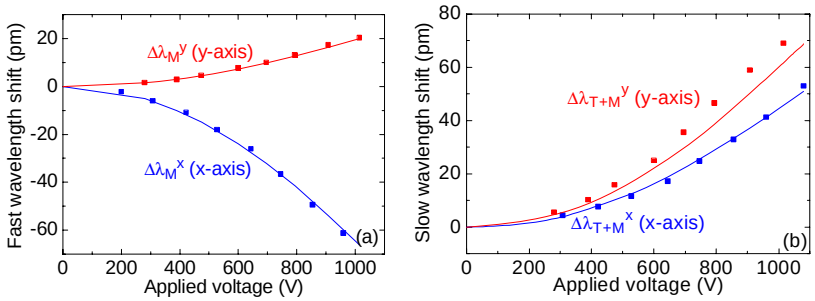

Fig. 3. (Color online) Experimental data (squares) and numeric simulations (solid lines) of Bragg wavelength shift for a 241 ns electrical pulse. (a) Fast wavelength shift for both polarization states measured at instant t_1. (b) Slow wavelength shift measured at instant t_3.

3. Simulation

To better study the physics of the Bragg wavelength shift for both polarizations, the partial differential equations describing heat diffusion and displacement in x and y-direction were solved by the finite element technique using the commercial software FlexPDE. The solutions allowed finding the time-dependent strain components in the fiber in the x- and y-directions (ε_x and ε_y), the temperature distribution over the core and to calculate the FBG wavelength shift in x- and y-polarizations according to the following formula [14-15]:

$$\Delta\lambda_x = -\lambda_x \frac{n_0^2}{2}\left(p_{11}\varepsilon_x + p_{12}\varepsilon_y\right) + \lambda_x(\alpha+\xi)\Delta T \quad (1)$$

$$\Delta\lambda_y = -\lambda_y \frac{n_0^2}{2}\left(p_{11}\varepsilon_y + p_{12}\varepsilon_x\right) + \lambda_y(\alpha+\xi)\Delta T \quad (2)$$

where: λ_x=1547.23nm, λ_y=1547.273nm are the initial Bragg wavelength for x- and y-polarizations; $n_0 = 1.445$ is the initial effective refractive index of the core; $p_{11} = 0.121$ and $p_{22} = 0.270$ are the photoelastic coefficients of the fiber [16]; α is the thermal expansion coefficient of silica; $\xi = (1/n)(dn/dT) = 6.5\times10^{-6}$ K^{-1} is the thermo-optic coefficient of fused silica; ΔT is the increased temperature in the core. The first terms of Eqs. (1) and (2) stand for the wavelength shift of both polarizations due to mechanical stress in the core, while the second terms of two equations indicates the wavelength shift caused by the increased temperature in the core.

Stress at the BiSn/cladding boundary increase approximately linearly during the electrical pulse action, and then gradually decrease with time. This stress is transferred to the core area in ~14 μm/5720 m/s = 2.45 ns, i.e. almost instantaneously compared to the pulse duration 241 ns. However, the heat at the BiSn/cladding interface needs several microseconds to reach the core area. As a result, the heat diffusion can be neglected during the pulse action. The fast wavelength shifts $\Delta\lambda_M^x$ and $\Delta\lambda_M^y$ are determined by the first terms of Eqs. (1) and (2) at t = 241 ns. The exact value of the heat capacity and the expansion coefficient of the BiSn alloy electrode are not known, nor the exact heat capacity for the Ge-doped silica fiber used. The choice C_v = 167 J/kgK and $\Delta l/l = 15.5\times10^{-6}$ K^{-1} for the alloy and C_v = 736 J/kgK for the fiber allowed for excellent fitting of the theoretical equations (1) and (2) to the experimental data, as seen in Fig. 3(a). The simulations confirm that the core area is compressed (negative) in x-direction and stretched (positive) in y-direction under the applied pulses. For the pulse with applied voltage 1080 V, $\varepsilon_x = -1.655\times10^{-4}$ and $\varepsilon_y = 2.535\times10^{-4}$ at t = 241 ns. This results in a decrease of refractive index in x-direction (-7.3×10^{-5}) and a weaker increase of refractive index in y-direction ($+2.11\times10^{-5}$), corresponding to $\Delta\lambda_M^x$ = -75.8 pm and $\Delta\lambda_M^y$ = +23.7 pm. We can conclude (in opposition to [9, 12]) that the fast axis mode is in the direction parallel to the two holes (x-direction), and the slow axis mode is in the direction orthogonal to the two holes (y-direction).

#94010 - $15.00 USD Received 18 Mar 2008; revised 19 May 2008; accepted 19 May 2008; published 21 May 2008

As mentioned above, the slow wavelength shift is caused by the relaxation of mechanical stress and the increased temperature in the core. It can be calculated from Eqs. (1) and (2) for both polarizations. For the x-polarization, $\Delta\lambda_x$ equals zero at a calculated time t_2 = ~56 μs, when the two terms of Eq. (1) compensate each other. Subsequently, the second term dominates and $\Delta\lambda_x$ becomes positive and increases gradually due to the increasing ΔT. The shift reaches its maximum at a calculated time t_3 = ~250 μs. For the y-polarization, initially $\Delta\lambda_y$ reduces because the decay of the stress dominates over the rising effect of heat. At a calculated time t_2 ~17 μs the latter starts to dominate and the shift increases again until it reaches the maximum value at a calculated time t_3 ~ 200 μs.

The simulations of $\Delta\lambda_{T+M}^{x}$ accurately reproduce the experiment measurements when the thermal expansion coefficient for the silica fiber is optimized to the value $\alpha = 0.50\times10^{-6}$ K^{-1}. This is shown by the blue line and squares in Fig. 3(b). The simulation of the wavelength shift for the y-axis now has no free parameters for adjustment. The result (red line in Fig. 3(b)) fits the experimental data (squares) relatively well. The numerical predictions are smaller than the measured values. The small discrepancy could possibly be attributed to a temperature variation taking place during the measurement. For example, the difference between the calculated and measured $\Delta\lambda_{T+M}^{y}$ at the pulse voltage 1015 V corresponds to a temperature shift of 0.8 °C, well within the temperature uncertainty in the laboratory, which could have been rising during the measurement.

The complete simulations here agree well with a simple quadratic fit to the data for $\Delta\lambda_M$ and $\Delta\lambda_{T+M}$ (for both polarizations) as a function of the pulse voltage [12].

Figure 4 illustrates the simulation results of the time evolution of the temperature in the core center under different pulse excitation. The voltages shown in Fig. 4 are obtained multiplying the applied voltage by 2×43/(43+50) to take into account the impedance mismatch between the device and the 50 Ω coaxial cable. As shown in Fig. 4, the heat in the metal takes ~10 μs to reach the core and increases to the maximum at ~190-220 μs. Note that the maximum ΔT in the metal is as high as ~90 °C for a corresponding core temperature increase of only ~6.2 °C.

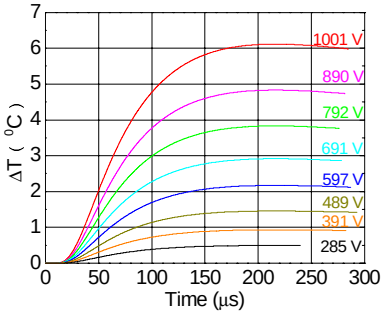

Fig. 4. (Color online) Simulation results of the time evolution of the temperature in the center of the core under different voltage pulse excitation.

4. Conclusion

A FBG was written in a side-hole fiber with internal metal alloy electrodes, resulting in two reflected peaks separated by 43 pm due to the intrinsic geometrical birefringence. Nanosecond risetime current pulses of up to 23 A were applied to the metal electrode, which heated and expanded rapidly. On a nanosecond scale, the fast Bragg wavelength shift of the fast axis mode is negative and that of the slow axis mode is positive and smaller, because of the mechanical perturbation. Microseconds later, the relaxation of the mechanical stress and the effect of heat reaching the core red-shift both Bragg peaks. All wavelength shifts depend quadratically on the electrical pulse voltage. Numerical simulations were developed to accurately and quantitatively explain the experimental observations. Similar components to the one used here have been tested to 10^9 pulses without degradation of performance [17].

#94010 - $15.00 USD Received 18 Mar 2008; revised 19 May 2008; accepted 19 May 2008; published 21 May 2008

This component has potential applications for Q-switching fiber lasers and RF signal generation.

#94010 - $15.00 USD Received 18 Mar 2008; revised 19 May 2008; accepted 19 May 2008; published 21 May 2008